

Using the complex Jacobi method to simulate Kerr non-linear photonic components

PETER VANDERSTEEGEN*, BJORN MAES, PETER BIENSTMAN
AND ROEL BAETS

Department of Information Technology, Ghent University-IMEC, St.-Pietersnieuwstraat 41, 9000 Ghent, Belgium

*(*author for correspondence: E-mail: Peter.Vandersteegen@intec.UGent.be)*

Received 30 September 2005; accepted 31 January 2006

Abstract. The iterative complex Jacobi technique has been extended to simulate the third order Kerr effect in wavelength scale dielectric structures. This method solves the Helmholtz equation in a discrete finite simulation space by an iterative process. An update equation refines the field values at each iteration step, until a desired accuracy is achieved. We have extended the iterative process with an extra calculation step which allows simulating materials with the non-linear third order Kerr effect. Our adjustment of the discrete field operators in the update equation also introduces PMLs as absorbing boundaries and the total field/scattered field formalism as field source for this method.

Key words: central differences, complex Jacobi iteration, Helmholtz equation, Kerr effect, PML, total field/scattered field

1. Introduction

In this paper several improvements to the recently introduced complex Jacobi (CJ), (Hadley 2005) technique are discussed. The proposed extensions allow modeling of dielectric structures with the instantaneous non-linear Kerr effect. This Kerr effect is modelled as an intensity dependent refractive index. High intensity is achievable by increased confinement of light in advanced dielectric structures, e.g. photonic crystals and photonic wires. The fabrication of these structures has been made possible by recent advanced production techniques.

Finite Difference Time Domain (FDTD), (Taflove 1995), Beam Propagation (BPM), (Burzler *et al.* 1996) and eigenmode expansion (EME), (Maes *et al.* 2005) are able to simulate a wide variety of non-linear dielectric wavelength scale components. FDTD gives insight in the time-evolution of the fields by numerically integrating Maxwell's equations in the time domain. A steady state solution however requires all transient fields to be extinct. The extinction rate of these transient fields is completely dependent on the reflections in the structure. BPM only gives an accurate solution for the steady state fields if reflections are negligible. The lack of bidirectionality is

a limiting assumption. EME is a bidirectional frequency domain method. Its main application area are dielectric structures which consist of a few z -invariant sections.

We propose several extensions of the complex Jacobi method, a general frequency domain method which numerically integrates the central difference equivalent of the Helmholtz equation. Bidirectionality is automatically implied by the Helmholtz equation. There is also no assumption of z -invariance. The found field-amplitudes are located on an equidistant mesh. These amplitudes are invariant in time, save a phase factor.

Our improvements allow modeling of general non-linear components. Good absorption at the boundaries is achieved by extending the method with perfectly matched layers (PML). We inject a field profile in the simulation area by an adjusted total field/scattered field formalism (TFSF). The PML and TFSF extensions are respectively based on (Chew and Weedon 1994) and (Taflove 1995). Although the basic complex Jacobi method is a fully vectorial solver in 3 dimensions, the proposed extensions have only been tested for the scalar 2D Helmholtz equation.

In Section 2 we will give an overview of the linear extensions for the complex Jacobi method, such as PML and TFSF. In Section 3 we will introduce the non-linear extension. A quantitative comparison of the proposed simulation technique has been made with non-linear EME in Section 4. Another example, a propagating soliton in homogeneous space, is discussed in Section 5.

2. Linear complex Jacobi Method

The basic complex Jacobi method (Hadley 2005) is an iterative method which solves the Helmholtz equation on a mesh. Only the fields at equidistant points are calculated. The derivatives in the Helmholtz equation are replaced by central differences:

$$\frac{\partial}{\partial x} e_{i,j} \equiv \frac{e_{i+1,j} - e_{i-1,j}}{2\Delta x} \quad (1)$$

The field $e_{i,j}$ is located at the point $(i\Delta x, j\Delta y)$, i and j are integers, Δx and Δy are the discretization steps in x and y directions. This gives us the following scalar Helmholtz equation for a discrete mesh:

$$\begin{aligned} \nabla^2 e_{i,j} + k^2 e_{i,j} &= \left(\frac{\partial^2}{\partial x^2} + \frac{\partial^2}{\partial y^2} + (k_0 n_{i,j})^2 \right) e_{i,j} \\ &= 0 \end{aligned} \quad (2)$$

$$\begin{aligned}
 n_{i,j} &= n(i \Delta x, j \Delta y) \\
 k_0 &= \frac{2\pi}{\lambda_0}
 \end{aligned} \tag{3}$$

The wavelength in free space is λ_0 , $n_{i,j}$ is the position dependent refractive index.

The two step iteration process refines the fields with a correction factor until a desired accuracy has been achieved.

$$e_{i,j}^{n+1} = e_{i,j}^n + \left(2\alpha_1 \left(\frac{1}{\Delta x^2} + \frac{1}{\Delta y^2} \right) \right)^{-1} \left(\left(\delta_x^2 + \delta_y^2 + \left(\frac{2\pi}{\lambda} n_{i,j} \right)^2 \right) e_{i,j} \right) \tag{4}$$

The superscript n is the iteration step. The iteration process consists of repeatedly updating the fields with this equation, firstly with α_1 , then with α_2 , until a desired accuracy is achieved.

Using $\exp(-j\omega t)$ as convention for the time dependent phase factor of the invariant field amplitudes results in the following optimal constants: $\alpha_1 = \sqrt{3} - 1j$ and $\alpha_2 = -\alpha_1^*$. Derivation of these optimal values for α_1 and α_2 can be found in the original paper (Hadley 2005).

The implementation of the TFSF and PMLs results in the simulation area of Fig. 1. The photonic structure under investigation is placed in the total field region. These extensions are respectively described in subsection 2.1 and 2.2.

2.1. TOTAL FIELD/SCATTERED FIELD

The TFSF formalism allows to inject a desired wave in the simulation space. Figure 1 demonstrates how the scattered field/total field interface

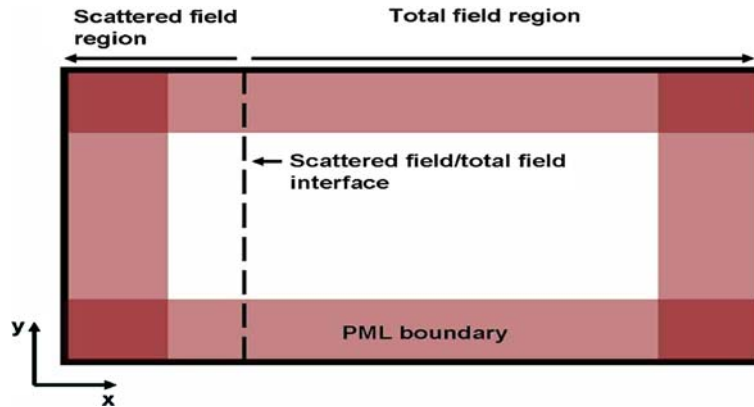


Fig. 1. A simulation box with 'total field/scattered field' as field source and PMLs as absorbing boundary conditions.



Fig. 2. Interface between scattered field–total field.

injects the desired field profile in the total field region. In the scattered field region only the scattered field, i.e. the total field without the exciting field is calculated.

Equation 4 allows us to calculate $e_{(i',j),\text{tot}}^n$ in the total field region, $e_{(i',j),\text{scatt}}^n$ in the scattered field region. The use of the update equation in the scattered field region implicitly assumes superposition of exciting field and scattered field. This also implies the exciting field is a solution for the discretized Helmholtz equation and the scattered field region consists of linear materials. Non-linear materials have to be located in the total field region.

The calculation of an amplitude at the interface between the regions is illustrated by Fig. 2.

$$\begin{aligned} e_{(i'-1,j),\text{scatt}}^n &= e_{(i'-1,j),\text{tot}}^n - e_{(i'-1,j),\text{source}} \\ e_{(i',j),\text{tot}}^n &= e_{(i',j),\text{scatt}}^n + e_{(i',j),\text{source}}, \quad \forall n, \forall j \end{aligned} \quad (5)$$

The injected field amplitudes $e_{(i'-1,j),\text{source}}$ and $e_{(i',j),\text{source}}$ are the amplitudes of the exciting wave at respective positions $(i' - 1, j)$ and (i', j) . Substituting Equation (5) in the update Equation (4) in order to calculate $e_{(i'-1,j),\text{scatt}}^n$ and $e_{(i',j),\text{tot}}^n$ gives the required update equations. The following equations have omitted the j -index of the y -direction for simplicity.

$$\begin{aligned} e_{i'-1,\text{scatt}}^{n+1} &= e_{i'-1,\text{scatt}}^n \\ &\quad + C \left(\frac{e_{i',\text{tot}}^n - e_{\text{source},i'} + e_{i'-2,\text{scatt}}^n - 2e_{i'-1,\text{scatt}}^n}{\Delta x^2} - k^2 e_{i'-1,\text{scatt}}^n \right) \\ e_{i',\text{tot}}^{n+1} &= e_{i',\text{tot}}^n + C \left(\frac{e_{i'+1,\text{tot}}^n + e_{i'-1,\text{scatt}}^n + e_{\text{source},i'-1} - 2e_{i',\text{tot}}^n}{\Delta x^2} - k^2 e_{i',\text{tot}}^n \right) \\ C &= \left(2\alpha \left(\frac{1}{\Delta x^2} + \frac{1}{\Delta y^2} \right) \right)^{-1} \end{aligned}$$

With these adjusted update formulae, it becomes possible to inject any desired field.

2.2. ABSORBING BOUNDARIES BASED ON PML

Elimination of reflections at the boundaries of a finite simulation box is necessary to achieve physical simulation results. Every wave incident on

these boundaries should be absorbed for any polarization and incident angle, without any spurious reflections. One of the most efficient absorbing boundaries is the Perfectly Matched Layer (PML). In this paper we report on the extension of the complex Jacobi method with a PML based on complex coordinate stretching (Chew and Weedon 1994). Complex Coordinate stretching results in the easiest implementation of PML for the complex Jacobi method.

The implementation of PMLs is based on adjusted difference operators in the absorbing boundary layer:

$$(\delta_x^2 + \delta_y^2)e = \frac{1}{s_x} \frac{\partial}{\partial x} \left(\frac{1}{s_x} \frac{\partial}{\partial x} e \right) + \frac{1}{s_y} \frac{\partial}{\partial y} \left(\frac{1}{s_y} \frac{\partial}{\partial y} e \right) \quad (6)$$

For $s_x = 1.0$ the previous formula reduces to the classical Helmholtz equation. A complex function s_x results in absorption in the x -direction, a complex function s_y results in absorption in the y -direction.

A finite difference equivalent of Equation (6) gives us:

$$\begin{aligned} \delta_x^2 e &= \frac{1}{s_x} \left(\frac{\partial}{\partial x} \frac{1}{s_x} \right) \frac{\partial}{\partial x} e + \frac{1}{s_x^2} \frac{\partial^2}{\partial x^2} e \\ &= \frac{1}{s_{x,i}} \left(\frac{\frac{1}{s_{x,i+1}} - \frac{1}{s_{x,i-1}}}{2\Delta x} \right) \left(\frac{e_{i+1} - e_{i-1}}{2\Delta x} \right) + \frac{1}{s_{x,i}^2} \frac{e_{i+1} + e_{i-1} - 2e_i}{\Delta x^2} \end{aligned}$$

In our experience, optimal absorption was achieved with linearly increasing PML from $s_x = 1.0$ to $s_x = 1.0 + 0.75j$ over 30 grid-points. These complex coordinates implicitly assume the time dependant phase factor of the amplitudes is $\exp(-j\omega t)$.

3. Extending the iterative process to simulate Kerr non-linearities

Simulating structures with the instantaneous Kerr effect can be modeled with an extra extension besides TFSF and PML. The basic idea is an extra update-step of the refractive index after each iteration step. The instantaneous Kerr effect is modeled by $n = n_{\text{lin}} + n_2 |E|^2$. This formula for the spatially dependent refractive index can be transformed in the following update equation:

$$\epsilon_{i,j}^n = (n_{i,j,\text{lin}} + n_{i,j,2} |e_{i,j}|^2)^2 \quad (7)$$

This equation is used in combination with the iteration process, described in Equation (4). After each iteration step, the field at a certain location results in an adjusted refractive index.

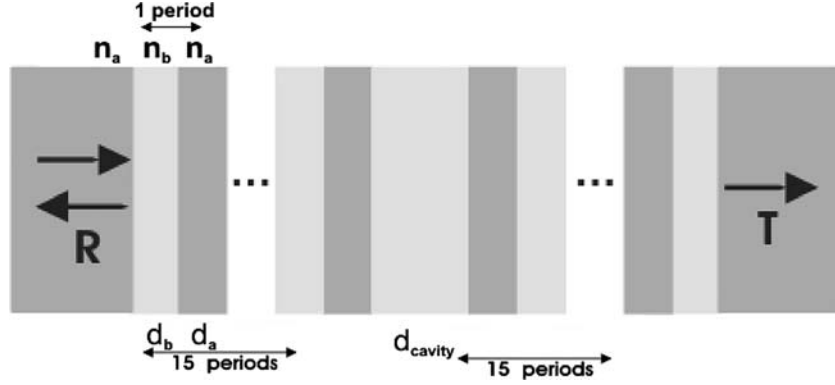


Fig. 3. Two Bragg mirrors encapsulate a cavity. ($\lambda_{\text{resonance}} = 1.56 \mu\text{m}$).

Validation of this principle has been done by comparing with nonlinear eigenmode expansion, as described in (Maes *et al.* 2005). The first simulation test setup consists of a resonant cavity for both the linear and non-linear case. The simulation time needed by both methods is also discussed. The end of this section also addresses the influence of the discrete mesh. The second simulation test setup shows the calculation of a soliton in free space.

4. Comparison with non-linear eigenmode expansion

Comparison with eigenmode expansion (EME) has been done by simulating the 1-dimensional structure of Fig. 3. The refractive indices in this setup are $n_a = 2.6$ and $n_b = 2.36$. The distances d_a , d_b and d_{cavity} are respectively $\lambda_{\text{resonance}}/4n_a$, $\lambda_{\text{resonance}}/4n_b$ and $\lambda_{\text{resonance}}/2n_b$. This structure is basically a cavity encapsulated by two Bragg mirrors.

The cavity causes a resonance peak in the middle of the bandgap, as illustrated in Fig. 4. A non-linear material in the central cavity causes a shift of the central resonance wavelength to a higher wavelength. Figure 5 illustrates this behaviour. The incoming plane wave has an amplitude $e = 1 \frac{V}{m}$. The non-linear cavity uses $n_2 = 5 \cdot 10^{-3} \frac{m^2}{V^2}$, n_2 as defined in formula 7. Figure 5 also illustrates a good agreement between the results calculated by EME and the results calculated by the complex Jacobi method (CJ).

Another point under discussion is the simulation time. EME has an advantage if large sections of the simulation space can be modeled as linear. When using EME, these linear sections only need to be calculated once. EME uses an iterative process for the non-linear sections, which results in the re-calculation of the eigenmodes in these sections for every

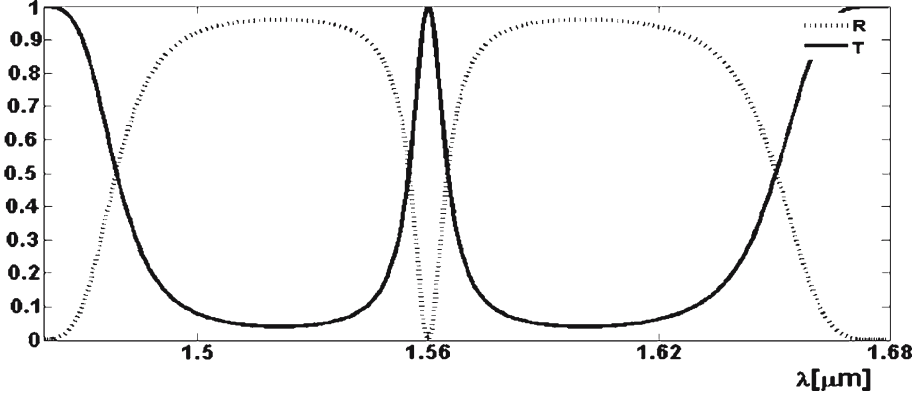


Fig. 4. Power transmission and reflection, see structure in Fig. 3.

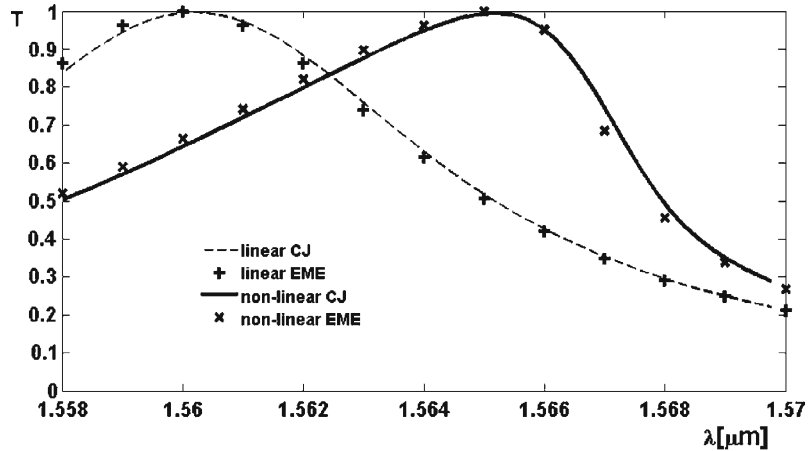


Fig. 5. Power transmission for linear and non-linear cavity. ($\Delta x = 15$ nm).

iteration. This quickly becomes a bottleneck when increasing the amount of non-linear sections.

Convergence of our method is guaranteed even for an extremely large non-linearity of $n_2 = 0.025 \frac{m^2}{V^2}$ with the previously described simulation parameters. This results in an increase of refractive index of approximately $\Delta n \approx 0.6$. We did not notice a significant decrease of convergence rate for these large non-linearities in this setup.

Therefore, our proposed extension to CJ is very well suited for structures where the non-linearity is present in a large portion of the simulation domain. In such a situation EME would not be very efficient.

Simulating the steady state solution of the previous problem with a time domain simulation method – e.g. FDTD – would require extremely long

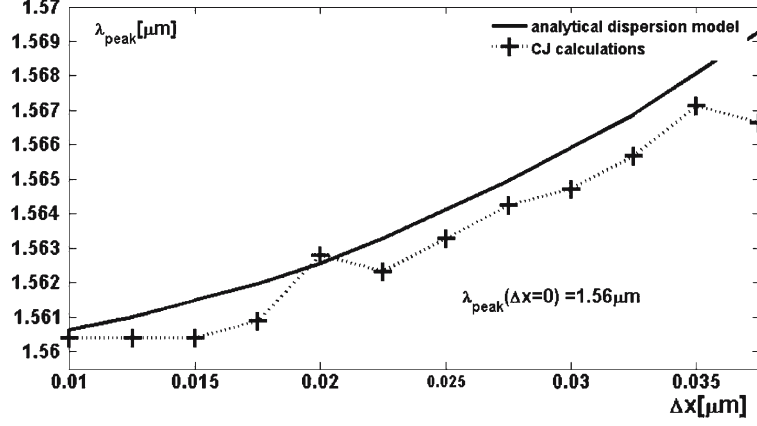


Fig. 6. Resonance peak -cfr. Fig. 3- shifts in function of the discretization step. (The analytical dispersion model uses Equation (8) to adjust n_a and n_b in the calculated structure.).

simulation times. This is especially the case for a structure with many reflections, as is the case for this example. The bidirectionality of the component eliminates BPM as a simulation tool.

4.1. INFLUENCE OF DISCRETIZATION STEP

A coarse grid for simulating the *linear* structure of Fig. 3 results in a resonance peak shift to higher wavelengths, as can be seen in Fig. 6. The ‘analytical dispersion model’ curve calculates the shift of the resonance peak by only taking into account numerical dispersion. The effective refractive index $-n_{eff} = \frac{\omega c}{k_0}$, ‘felt’ by a plane wave in a discrete simulation space is different than the actual refractive index. Based on Fig. 6 we can conclude that the shift is mostly caused by numerical dispersion.

The analytical dispersion model ignores the staircase phenomena which is caused by only taking into account the refractive indices at an integer $(\Delta x, \Delta y)$. This is also an intrinsic property of a discrete mesh.

The analytical dispersion model curve calculates the resonance peak of Fig. 3 with the effective refractive indices $n_{eff,a}$ and $n_{eff,b}$. These effective refractive indices are calculated with the dispersion relationship of plane wave in a homogeneous wave.

$$\frac{4 \sin^2 \left(\frac{k_0 n_{eff} \Delta x}{2} \right)}{\Delta x^2} = \frac{\omega^2}{c^2}$$

$$n_{eff} = \frac{\arcsin \left(\frac{k_0 \Delta x}{2} \right)}{\frac{k_0 \Delta x}{2}} \quad (8)$$

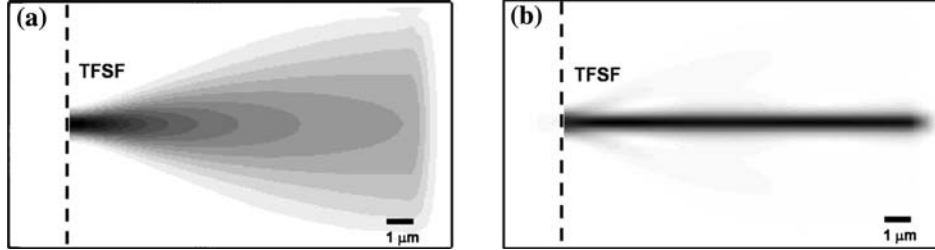


Fig. 7. Injection of a gaussian field profile in a linear and non-linear medium. ((a): diffraction in linear medium, (b): soliton in non-linear medium).

For a small value formulae 8, n_{eff} reduces to the refractive indices in continuous space: $n_{eff} = n$.

5. Spatial soliton in a non-linear Kerr-material

We have validated our extensions by simulating the self-focusing of a gaussian beam in non-linear space. In linear space, the injection of a Gaussian field profile by the total field/scattered field formalism results in a diffraction pattern. Both effects can be seen in Fig. 7. The Gaussian field profile is described by $e = 1.0 e^{-\frac{x^2}{2 \cdot 0.25^2}} \frac{V}{\mu\text{m}}$. The material is described by the refractive index $n = 3.6$ and $n_2 = 0.2 \frac{m^2}{V^2}$.

Eigenmode Expansion would require a large amount of eigenmodes to simulate the same straight forward simulation setup. The lack of linear regions, which should only be calculated once, takes away the main advantage of non-linear EME.

6. Conclusion

Our extensions to the recently introduced complex Jacobi method allow the simulation of 2D-components with Kerr-based materials in the frequency domain. Our proposed extension to the complex Jacobi method is very well suited for structures where the non-linearity is present in a large portion of the simulation domain.

Acknowledgements

Bjorn Maes and Peter Bienstman acknowledge the Flemish Fund for Scientific Research (FWO-Vlaanderen) for their postdoctoral fellowships. Parts

of this work were performed in the context of the Belgian DWTC project IAP-Photon.

References

- Burzler, J.M., S. Hughes and B.S. Wherrett. *Appl. Phys. B* **62**(4) 389, 1996.
Chew, W.C. and W.H. Weedon. *Microwave Opt. Tech. Lett.* **7** 599, 1994.
Hadley, R.G. *J. Comput. Phys.* **203**(1) 358, 2005.
Maes, B., P. Bienstman and R. Baets. *Opt. Quan. Electron.* **36**(1–3) 15, 2005.
Taflov, A. *Computational Electrodynamics The Finite-Difference Time-Domain Method*, Artech House, Boston-London, 111–117, 1995.